Hybrid materials based on azopolymer and sol-gel synthesized silver-containing titanium oxide nanoparticles with photoinduced birefringence

Raquel Fernández*, Junkal Gutierrez, Arantxa Eceiza and Agnieszka Tercjak*

The main goal of this work was the development of novel nanocomposite films with different optical properties. A non-toxic water soluble azopolymer was modified with TiO_2 nanoparticles and silver-containing TiO_2 nanoparticles. The thermal stability and glass transition temperature were enhanced in the silver-containing hybrid materials. Birefringence can be optically induced and erased in the azopolymer and the nanocomposites with and without silver. However, the photoorientation rate and the maximum and remaining birefringence values varied depending on the concentration of azopolymer in the nanocomposites and the presence of silver-containing nanoparticles. In nanocomposites with low concentration of azopolymer the presence of silver in the nanocomposite films improved dramatically the induced birefringence level. Moreover, the semiconductive properties of the developed hybrid materials were studied by electrostatic force microscopy, applying both positive and negative voltage.

1. Introduction

Azobenzene chromophores have been widely used as dyes and pH indicators for years, but in the past decades azobenzene-containing polymers or azopolymers have attracted considerable attention in material science and technology for their fascinating stimuli-responsive properties. Key to some of their most interesting applications is the reversible photoinduced isomerization between *trans* and *cis* isomeric states that azobenzene chromophores undergo upon exposure to light. The formation of *cis* isomers leads to remarkable changes of size, dipole moment, and geometry of azobenzene molecules. In addition, azobenzene compounds have the ability to photoorientate through optical induced *trans-cis-trans* isomerization cycles, which gives rise to birefringence and dichroism in azopolymers.[1-3]

The main applications of azopolymers include reversible optical storage, which relies on the possibility of altering their refractive index by means of light. A single domain could encode one bit by either being isotropic or birefringent, a difference that is easily probed optically.[4-7] Another intriguing application is the photoinduced bending of azobenzene-containing polymer films. Yu *et al*.[8] showed that a film of azopolymer could be repeatedly and precisely bent along any chosen direction by using linearly polarized light. In drug delivery applications using azobenzene compounds, light can be used to control the loading-unloading of small molecule drugs. The properties of surfaces modified with azobenzene groups can be also optically manipulated. Ichimura *et al.*[9] reported the photoinduced macroscopic motion of liquids on a flat solid surface covered by a photoisomerizable monolayer containing azobenzene units. Lim *et al.*[10] developed fluorinated azobenzene-modified nanoporous substrates that were photoreversibly converted between superhydrophobicity and superhydrophilicity as a result of photoirradiation, and Goulet-Hanssens *et al.*[11] developed a photoreversible cell culture substrate containing azobenzene groups, whose capacity to support cell growth could be altered using light.

In general, in order to achieve the desired properties and applications, it is important to study and control the induced isomerization and orientation processes of azobenzene groups in the developed materials, namely photoorientation kinetics, maximum and remaining birefringence levels, among others. Many studies have been carried out to enhance these parameters, such as optimizing the azobenzene molecule chemical structure,[12-14] its geometry,[15] irradiation light properties,[16] intermolecular interactions,[17] etc. Additionally, azopolymer properties can be tuned by the combination of distinct materials in the same matrix. In this respect, hybrid inorganic/organic materials containing metal or semiconductor nanoparticles are interesting due to their unique optical, electrical, magnetic, luminescent and catalytic properties.[18-20] In fact, it has been demonstrated that the introduction of noble metal nanoparticles into azopolymer matrices can enhance the responsive activity to light due to the localized surface plasmon resonance of these nanoparticles,[21-26] especially when the azopolymer is irradiated at a wavelength close to their maximum absorption.[27] In line with this, Wu *et al.*[28] reported the fabrication of silver nanoparticle/azopolymer nanocomposites, which formed an inorganic/organic network-like structure by interactions between the polymer matrix and the nanoparticles, and they found that the stability of the induced birefringence in the azopolymer was improved by the incorporation of the silver nanoparticles. Shen *et al.*,[29] however, showed that the interaction between silver nanoparticles and polymer plays an important role in application of the localized surface plasmon resonance effect. Experimental results revealed that the photoorientation behavior could be improved or worsened with the addition of silver nanoparticles depending on the azopolymer chemical structure.

One of the most typical methods used to generate inorganic nanoparticles is the sol-gel (SG) synthesis,[30-33] which involves the evolution of inorganic networks through the formation of a colloidal suspension (sol) and further gelation of the sol to form a network in a continuous liquid phase (gel).[34] The most commonly used precursors for the sol-gel process are alkoxides, such as titanium isopropoxide that was used in this study for generating TiO_2 nanoparticles. The simplicity and versatility are the main advantages of this method to design hybrid materials. Nevertheless, all variables must be rigorously controlled, since small changes in one parameter, such as temperature, pH, reaction time or concentration can drastically affect the results.[35]

In this work, the sol-gel method was used for the development of hybrid inorganic/organic nanocomposites based on a non-toxic water soluble azopolymer consisting of a poly(vinyl amine) backbone with an azo dye as side chain. Good dispersion of silver nanoparticles in the host azopolymer is necessary to achieve the desired improvement in optical properties. Indeed, one of the main problems that prevent these hybrid systems from real applications is how to fabricate homogenous azopolymer/nanoparticle nanocomposites with good processability and controllable concentration of noble metal nanoparticles.[28] To meet this requirement, silver-containing TiO_2 nanocomposites that consist of TiO_2 nanoparticles supporting well dispersed Ag nanoclusters were fabricated by adding $AgNO_3$ precursor to the pure oxide sol under stirring at room temperature. Thus, the azopolymer was modified both with both neat TiO_2 nanoparticles and silver-containing TiO_2 nanoparticles and the morphology and semiconductive and optical properties of the resultant hybrid materials were investigated using different advanced characterization techniques, paying special attention to the influence of the nanoparticles on the induced birefringence properties of the developed multifunctional materials.

2. Experimental part

2.1. Materials and sample preparation

The azopolymer, poly[1-[4-(3-carboxy-4-hydroxyphenylazo)benzenesulfonamido]-1,2-ethanediyl, sodium salt] (PCBS) with a molar mass of 369.327 g/mol, was supplied by Sigma-Aldrich and used as received. Titanium isopropoxide (TTIP), Ti[OCH(CH3)2]4, purchased from Sigma-Aldrich, was used as precursor to obtain TiO_2 nanoparticles. Isopropanol (IPA) and an aqueous hydrochloric acid (HCl) solution (37 %) were also supplied by Sigma-Aldrich.

The titanium sol-gel solution (TiSG) was prepared by mixing IPA (10 ml), TTIP (2.5 mmol) and HCl (2.5 mmol) and letting it stir overnight. This solution was divided into two equal parts and silver nitrate 0.1M was added (20µL AgNO3/mL TiSG solution) to one of them and let stir for 6 h. Both the neat sol-gel solution and the silver-containing titanium sol-gel solution (Ti/AgSG) were used to prepare two different series of nanocomposites. Different amounts of the sol-gel solutions were added to PCBS solutions (0.5 or 2 wt % in H2O) and stirred for 2 h to prepare the series of hybrid systems named as PCBS-TiSG (Table 1).

Table 1. Composition of the developed hybrid systems.

Sample	PCBS (%)	TiSG or Ti/AgSG solution (%)
PCBS	100	-
PCBS90-TiSG	90	10
PCBS80-TiSG	80	20
PCBS70-TiSG	70	30
PCBS60-TiSG	60	40
PCBS50-TiSG	50	50
PCBS40-TiSG	40	60
PCBS1.1-TiSG	1.15	98.85
PCBS0.7-TiSG	0.74	99.25
PCBS0.5-TiSG	0.50	99.50
PCBS0.3-TiSG	0.33	99.67
PCBS90-Ti/AgSG	90	10
PCBS80-Ti/AgSG	80	20
PCBS70-Ti/AgSG	70	30
PCBS60-Ti/AgSG	60	40
PCBS50-Ti/AgSG	50	50
PCBS40-Ti/AgSG	40	60
PCBS1.1-Ti/AgSG	1.15	98.85
PCBS0.7-Ti/AgSG	0.74	99.25
PCBS0.5-Ti/AgSG	0.50	99.50
PCBS0.3-Ti/AgSG	0.33	99.67

Similarly, different amounts of silver-containing sol-gel solution were added to PCBS solutions (0.5 or 2 wt % in H_2O) and stirred for 2 h to prepare the series of hybrid systems named as PCBS-Ti/AgSG (Table 1). An illustration of the nanocomposites preparation method is shown in Scheme 1.

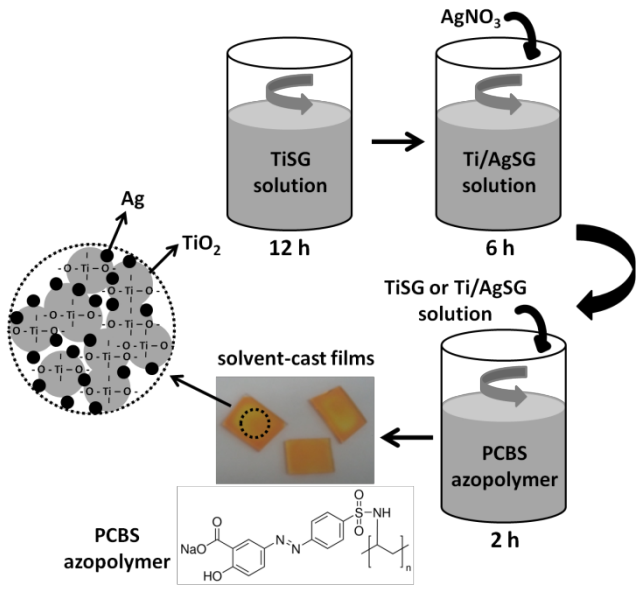

Scheme 1. Schematic illustration of the hybrid films preparation method.

Finally, all the solutions were filtered using a 0.2 μm nylon filter and films of all the nanocomposites were obtained by solvent-casting onto clean glass slides. Residual solvent was removed by evaporation at room temperature for 24 h and, then, under vacuum another 24 h.

2.2. Techniques

Thermogravimetrical analysis (TGA) of the samples was carried out using a TGA/SDTA-851e equipment under air atmosphere at a heating rate of 10 ºC min^{-1} from 25 to 900 ºC.

Differential scanning calorimetry (DSC) measurements were performed with a Mettler Toledo DSC 192 822 differential scanning calorimeter equipped with a sample robot 193 TSO 801 RO to measure the glass transition temperature (T_g) of the samples using a heating rate of 20 ºC min^{-1} from 25 to 250 ºC. Nitrogen was used as purge gas. All T_g values were taken at the onset of the change in specific heat.

Ultraviolet-visible (UV-Vis) absorption spectra of films deposited onto clean glass slides were recorded with a UV-3600 UV-vis-NIR spectrophotometer from Shimadzu.

Infrared spectra of the samples were taken using a Nicolet Nexus 670 Fourier transform infrared (FTIR) spectrometer equipped with a single horizontal golden gate attenuated total reflectance cell (ATR). Spectra were recorded using a spectral width ranging from 600 to 4000 cm^{-1}, with 4 cm^{-1} resolution and an accumulation of 32 scans.

The morphology of the samples was studied by atomic force microscopy (AFM). AFM images were obtained with a Nanoscope IIIa scanning probe microscope (Multimode™, Digital Instruments). Tapping mode (TM) in air was employed using an integrated tip/cantilever (125 µm in length with *ca* 300 kHz resonant frequency and spring constant of *ca* 40 N/m). Typical scan rates during recording were 0.7-1 line s^{-1} using a scan head with a maximum range of 16 µm x 16 µm.

Electrostatic Force Microscopy (EFM) was successfully employed to study the semiconductive properties of the nanoparticles in the design inorganic/organic nanocomposites. Measurements were performed in the Lift-Mode (lift height was 180-200 nm) in ambient conditions and EFM was equipped with an integrated Co/Cr coated MESP tip having a resonance frequency around 75 kHz. In order to obtain repeatable results of the investigated materials, different regions of the specimens were scanned.

Induced birefringence experiments were carried out at room temperature and under ambient conditions. The experimental setup used was similar to that previously reported.[36] Birefringence was induced in films of the azopolymer and the developed hybrid materials using a linearly polarized ultrashort pulse train at 488 nm (writing beam) with a polarization angle of 45º with respect to the polarization direction of a low power He-Ne laser operating at 632.8 nm (reading beam). Femtosecond laser pulses were generated by a Ti:Saphire oscillator-regenerative amplifier system (1 kHz, 4.0 mJ, 35 fs pulses @ 800 nm). The 488 nm radiation was produced by the sum frequency generation of the signal (1250 nm) of an optical parametric amplifier (OPA) and the 800 nm fundamental beam. The average power of the writing beam used in the experiments was 20 mW on a spot of 1.5 mm^2 and the change in the transmission of the reading beam, which passed through the sample between two crossed polarizers, was measured with a photodiode. Films were heated at 110 ºC for 10 min and subsequently stored at room temperature before experiments.

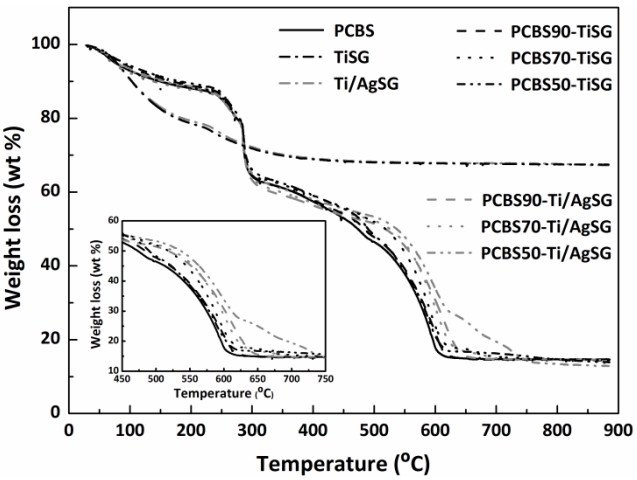

Fig 1. TGA curves of the developed hybrid systems at a heating rate of 10 ºC min^{-1}.

3. Results and discussion

Thermogravimetric curves of the developed hybrid systems containing different amounts of TiSG or Ti/AgSG are shown in Fig. 1. TGA plots of TiSG and Ti/AgSG exhibit a weight loss from almost the beginning of the experiment to around 400 ºC. This loss can be attributed to the release of water that was hydrogen-bonded to the TTIP precursor[37] and/or residual solvent.[38, 39]

From 400 to 900 ºC TGA curves remain constant, resulting in a net residue of 68 wt %. In the case of PCBS and the nanocomposites, the shape of the thermograms is very similar, indicating that the thermal degradation followed the same pathway. The weight loss up to approximately 300 ºC can also be ascribed to the release of water and/or residual solvent. Then, from 300 ºC to around 700 ºC the chemical decomposition of the organic part of the investigated systems takes place. The decomposition temperature of the nanocomposites is higher than that of the neat azopolymer and, in addition, it is shifted to higher values for silver-containing hybrid systems, especially for the sample with higher Ti/AgSG content. This can be related to strong interactions between the PCBS matrix and the sol-gel synthesized nanoparticles.[40-42] For all the samples a net residue of approximately 15 wt % was obtained.

The glass transition temperature of the samples was determined by DSC (Table 2). It was found that the T_g, which is 84 ºC for the neat azopolymer, decreased with the addition of TiSG from 81 ºC for 10 wt % of TiSG to 69 ºC for 50 wt % of TiSG. However, the addition of Ti/AgSG in PCBS matrix led to an increase in T_g up to 88 ºC for 50 wt % of Ti/AgSG. This can be attributed to stronger interactions between the silver-containing nanoparticles and the PCBS matrix, which also led to higher thermal stability of the nanocomposites with Ti/AgSG in agreement with TGA results.[43]

Table 2. Glass transition temperature of the developed hybrid systems.

Sample	T_g (ºC)
PCBS	84
PCBS90-TiSG	81
PCBS70-TiSG	77
PCBS50-TiSG	69
PCBS90-Ti/AgSG	85
PCBS70-Ti/AgSG	87
PCBS50-Ti/AgSG	88

The optical absorbance of the developed nanocomposites containing TiSG or Ti/AgSG was also investigated (Fig. 2). UV-Vis absorption spectra of films deposited onto clean glass slides were obtained in the range between 350-600 nm. The absorption maximum for PCBS appears at around 400 nm, which corresponds to the electronic transition of azobenzene groups, responsible for the photoisomerization. It is also well known that silver nanoparticles have a characteristic surface plasmon resonance band in the visible range.[44] As shown in Fig. 2, the optical absorbance at approximately 400 nm is higher for the silver-containing nanocomposites, indicating that the surface plasmon resonance band of silver nanoparticles might also be located at around 400 nm.

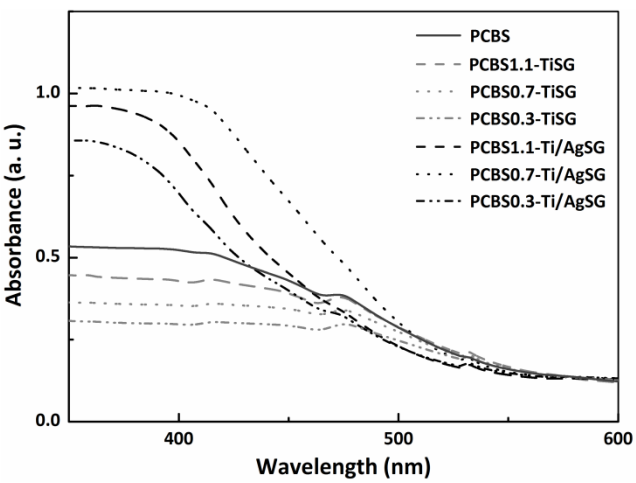

Fig. 2. UV-Vis absorbance of the developed hybrid systems.

FTIR spectra in the mid IR region, employed for the characterization of the developed hybrid materials, are shown in Fig. 3. No clear differences in the FTIR spectra of the samples were noted. In general, the band at around 3300 cm^{-1} corresponds to the stretching vibration of OH groups. The COOH stretching vibration band appears in the range between 1700-1500 cm^{-1} and the vibration associated with the stretching of N=N groups can be seen at around 1300-1400 cm^{-1}. Finally, in the range between 1200-1050 cm^{-1} appears the stretching vibration band of SO_2-NH groups.

The developed nanocomposite films morphology was investigated by atomic force microscopy. Fig. 4 shows AFM phase images of PCBS0.3-TiSG and PCBS0.3-Ti/AgSG systems.

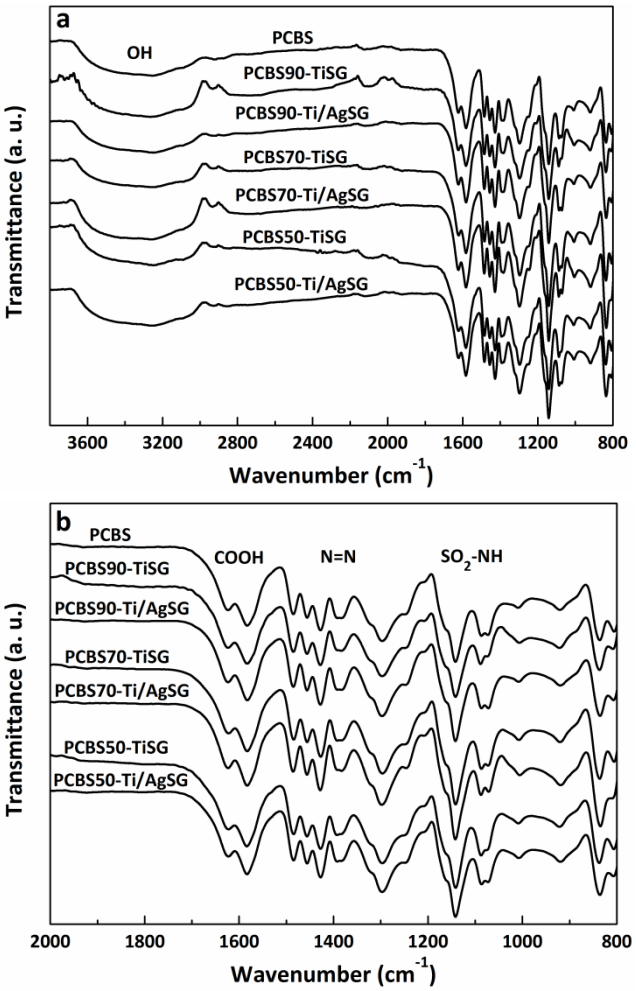

Fig 3. FTIR spectra of the developed hybrid systems.

The morphology of both films is clearly different, confirming that the modification of the titanium oxide nanoparticles with silver also had an effect on the nanocomposites morphology. The films of nanocomposites modified with silver-containing nanoparticles are more homogeneous and less rough than those without silver and, what is more, they show a nanostructured surface.

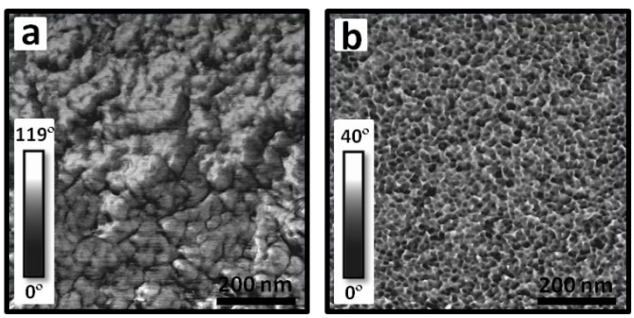

Fig. 4. AFM phase images (750 nm×750 nm) of: (a) PCBS0.3-TiSG and (b) PCBS0.3-Ti/AgSG.

In addition, semiconductive properties of the nanocomposites were studied by electrostatic force microscopy. EFM is a versatile technique for studying the electric field gradient distribution above the sample surface in order to distinguish different conductive parts

of the film since, when a voltage is applied to the tip, only charged domains of the sample surface are detected. In this case, the only components that can respond to the applied voltage in the investigated hybrid materials are the sol-gel nanoparticles, due to their semiconductive properties.

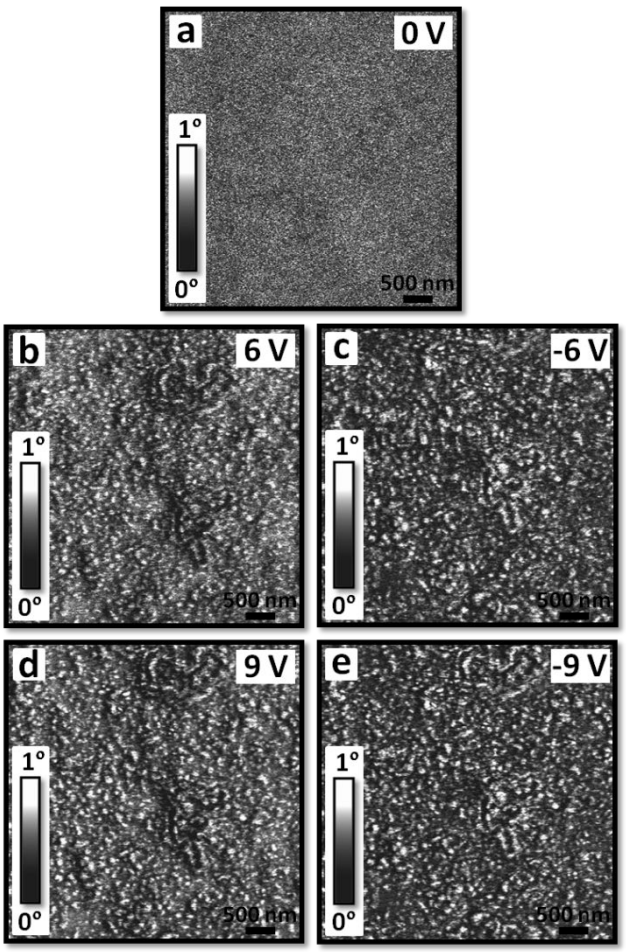

Fig. 5. EFM phase images (5 μm×5 μm) applying positive and negative voltage for PCBS0.3-SGAg system.

Fig. 5 shows EFM phase images obtained applying different positive and negative voltage. When a voltage of 0 V is applied to the tip, no charge domains are detected on the surface. Conversely, when a voltage (6 V or 9 V) is applied to the tip, bright domains appear on the sample surface, which correspond to the conductive nanoparticles, allowing us to clearly distinguish the charged and uncharged domains in the hybrid system. In addition, the response of the film to negative and positive voltages was also compared. Applying the same level of positive or negative voltage to the tip similar EFM phase images are achieved, which indicates that the sample is able to respond both to positive and negative voltage.

The induced birefringence properties of the developed multifunctional materials containing an azopolymer were also studied. Azobenzene molecules can be oriented by irradiation with linearly polarized light of appropriate wavelength. Upon absorbing this light, azobenzene groups undergo a series of *trans-cis-trans* isomerization cycles. Those molecules with dipole moment perpendicular to the polarization direction of the light electric field do not absorb light to undergo further isomerizations. At the end of several cycles, a net population of azobenzene groups is oriented in this perpendicular direction, leading to an induced birefringence in the film structure. The birefringence formation can be inferred by the change in transmittance of a probe beam that passes through the sample between crossed polarizers. To investigate the kinetics of azobenzene groups orientation in the nanocomposites, the creation of birefringence was monitored over time through three different irradiation regimes: when the linearly polarized orienting beam was turned *on* (A), after it was turned *off* (B) and, finally, when irradiated with circularly polarized light to randomize the induced orientation (C). The formation, relaxation and erasing of birefringence is illustrated in Fig. 6 by writing-relaxing-erasing sequences obtained for PCBS prepared from different concentrations in H_2O, 0.5 or 2 wt %.

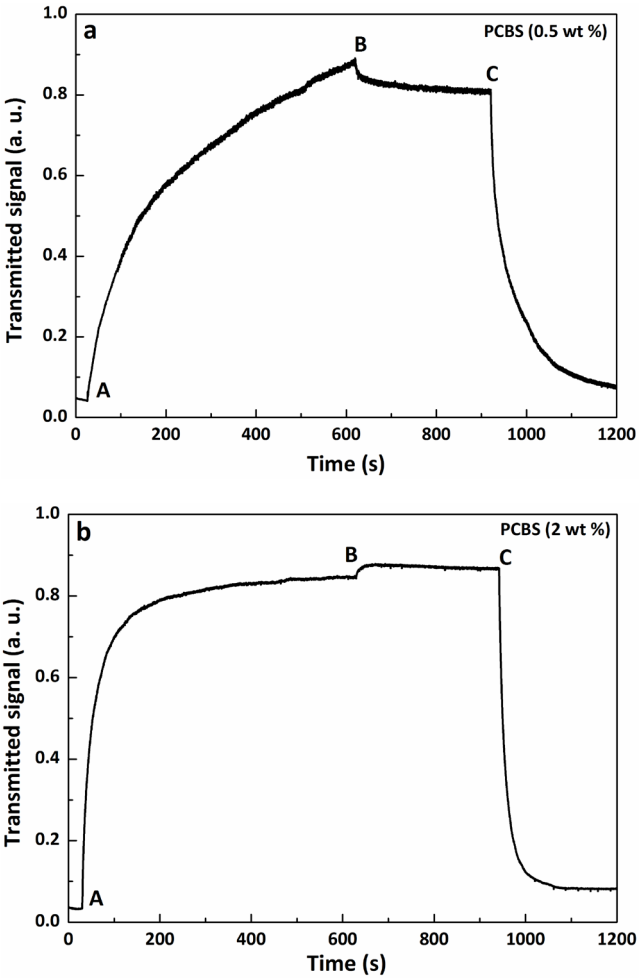

Fig. 6. Writing-relaxing-erasing cycles as a function of time for PCBS films obtained from different concentrations: (a) 0.5 wt % and (b) 2 wt % in H_2O.

The transmitted signal was normalized between 0 and 1. At the beginning of the experiment there is no transmission of the probe beam, since the azobenzene groups are randomly distributed. At point A, the pump beam is turned *on* and the probe beam is transmitted through the sample between crossed polarizers due to the birefringence induced in the film. However, the birefringence is built up faster to the saturation level for the most concentrated sample (2 wt %). Indeed, the time necessary to reach the maximum

level of birefringence is higher than 10 min for the sample obtained from 0.5 wt % solution in H_2O (Fig. 6a), much longer than the 3 min needed for the concentrated one (Fig. 6b). Taking into account that the transmitted signal is the result of photoinduced orientation of the azobenzene molecules, larger number of photoactive units in the films generates a higher birefringence and, consequently, a higher signal transmission. In addition, these results may be related to the increase in the writing beam absorption upon increasing azobenzene concentration.[45] The absorption increase can induce a sample heating, leading to a higher molecular mobility, which in this case might contribute to the orientation process. Furthermore, the increase of cooperative interactions among azobenzene units, as a consequence of the increase in azopolymer concentration in the films obtained from PCBS starting solution of 2 wt % in H_2O, can also help to stabilize the induced orientation.[7]

When the pump beam is turned *off* at point B, generally, as Fig. 6a shows, molecular relaxation takes place, giving rise to a stable birefringence pattern lower than the maximum induced value. Conversely, as observed in Fig. 6b, when the irradiation light is turned *off* an increase of induced birefringence in dark is observed. This response can be attributed to the increase of cooperative interactions among azobenzene units with increasing PCBS concentration and to the thermal *cis-trans* back isomerization.[46] When the pump beam is turned *off*, the *cis*-azobenzene concentration in the film will decay by thermal isomerization to the *trans* state. These *trans*-azobenzenes will be preferentially oriented by previously aligned azobenzene groups in films with higher azopolymer concentration thanks to mutual interactions among photoactive molecules.

Finally, at point C, in order to remove the remaining birefringence, circularly polarized light is introduced, which completely randomized the induced orientation in all cases.

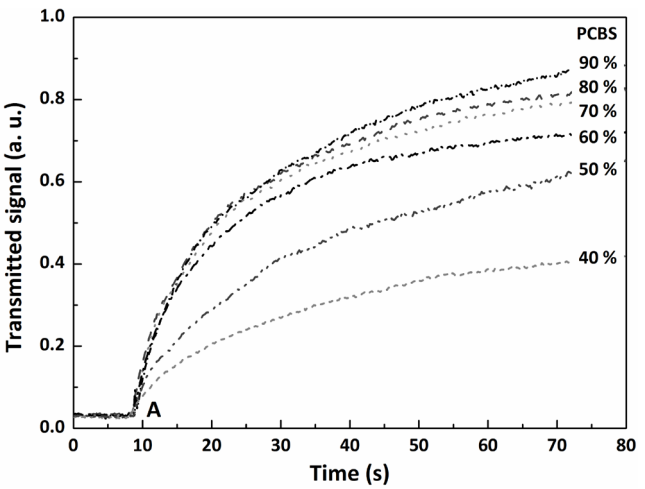

Fig. 7. Induced birefringence a function of time for the developed hybrid systems depending on PCBS content.

Fig. 7 shows the effect of the azopolymer content on the maximum transmitted signal in nanocomposites with different PCBS/TiSG ratios. There is an increase in the birefringence level as the azopolymer content increases. As discussed above, since birefringence is due to the photoinduced orientation of the azobenzene units, a larger number of photoactive molecules in the nanocomposite films generate a higher birefringence.

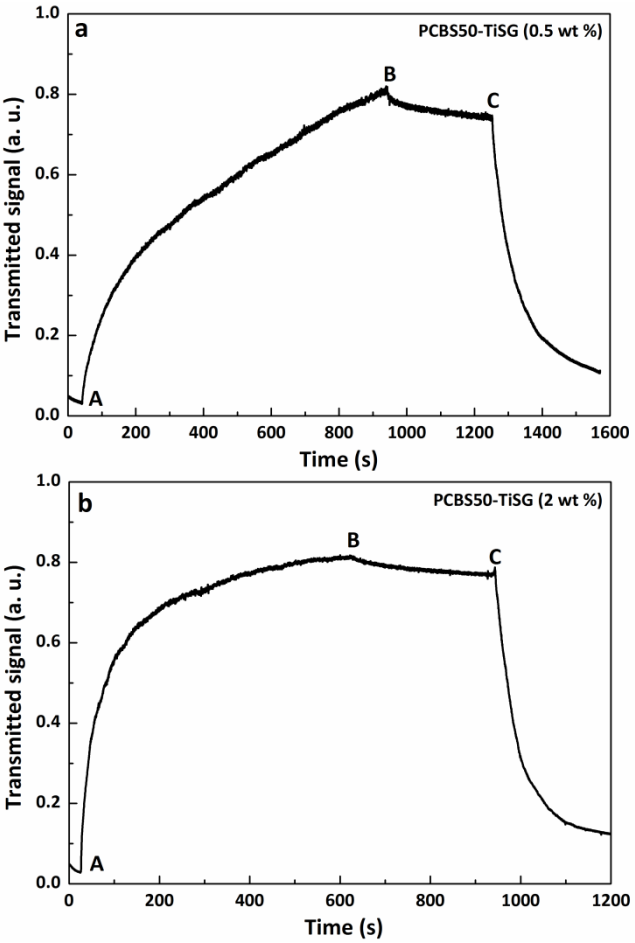

Fig. 8. Writing-relaxing-erasing cycles as a function of time for PCBS50-TiSG films obtained from different concentrations: (a) 0.5 wt % and (b) 2 wt % in H_2O.

The influence of the PCBS starting concentration was also evaluated in the developed hybrid systems (Fig. 8). In general, for the investigated nanocomposites it was observed that, similarly to the behavior exhibited by the neat PCBS, the photoinduced orientation rate and stability increased with increasing azopolymer concentration. However, although for the less concentrated systems (0.5 wt %) the birefringence decayed in all cases when turning *off* the irradiation light, for the most concentrated ones (2 wt %) the remaining birefringence after turning *off* the pump beam remained constant or slightly decreased, but it did not increased as in the case of neat PCBS. This result can be related to the fact that the presence of nanoparticles immersed in the azopolymer matrix might disrupt the interactions between azobenzene groups.

To finish, one of the main goals of this work was to investigate the influence of the silver-containing nanoparticles on the birefringent response of the samples. Fig. 9 shows writing-relaxing-erasing cycles obtained for nanocomposites with 10 wt % of TiSG or Ti/AgSG (Fig. 9a) and with 60 wt % of TiSG or Ti/AgSG (Fig. 9b) prepared from PCBS starting solution of 2 wt % in H_2O.

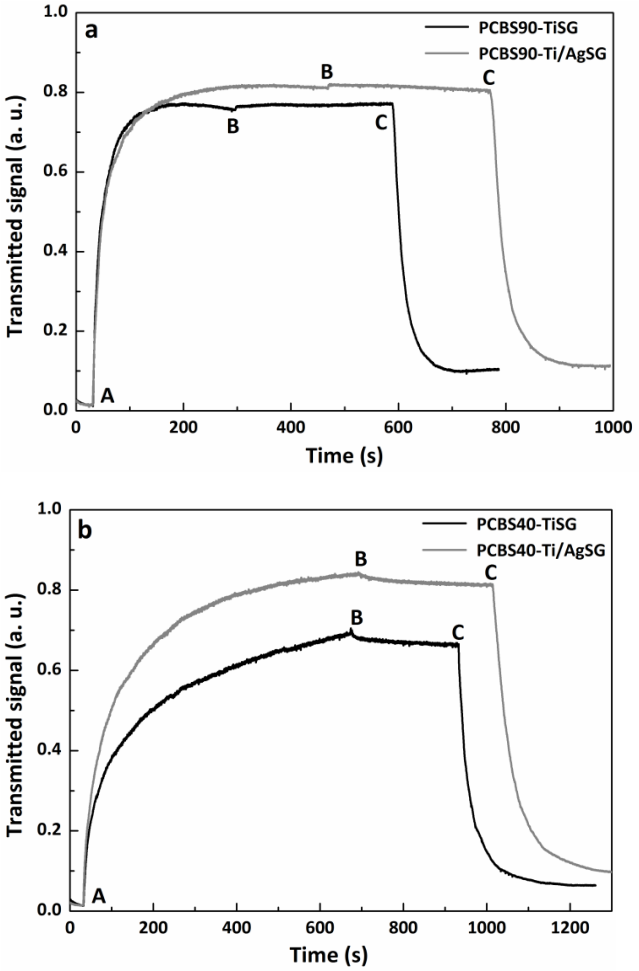

Fig. 9. Writing-relaxing-erasing cycles as a function of time for: (a) PCBS90-TiSG and PCBS90-TiAgSG, and (b) PCBS40-TiSG and PCBS40-Ti/AgSG.

The photoinduced orientation rate and the remaining birefringence increase with increasing PCBS content in the nanocomposites. In general, this behavior was exhibited by all the hybrid systems containing up to 60 wt % of sol-gel solution, but no clear differences were noted between the responses of the systems with TiSG or Ti/AgSG.

Fig. 10 shows writing-relaxing-erasing cycles as a function of time for systems with high content of sol-gel solution. Increasing significantly the amount of sol-gel solution in the samples, the maximum induced birefringence increases dramatically in the silver-containing films prepared from PCBS starting solution of 0.5 wt % in H_2O. For instance, in samples with PCBS content in the order of 1 wt % (Fig. 10a) the maximum induced birefringence is more than 3 times higher in the system with Ti/AgSG comparing to the one with TiSG. Decreasing PCBS content to 0.3 wt % (Fig. 10b), the maximum induced birefringence is more than 10 times higher in the silver-containing system comparing to the one with TiSG. Therefore, the induced birefringence of the investigated hybrid materials is strongly dependent on the presence of silver. This result may indicate that the silver-containing nanoparticles interacted with the azopolymer and the induced birefringence properties of the nanocomposites were enhanced, probably thanks to the surface plasmon resonance of silver nanoparticles at the wavelength of excitation of the azobenzene molecules.

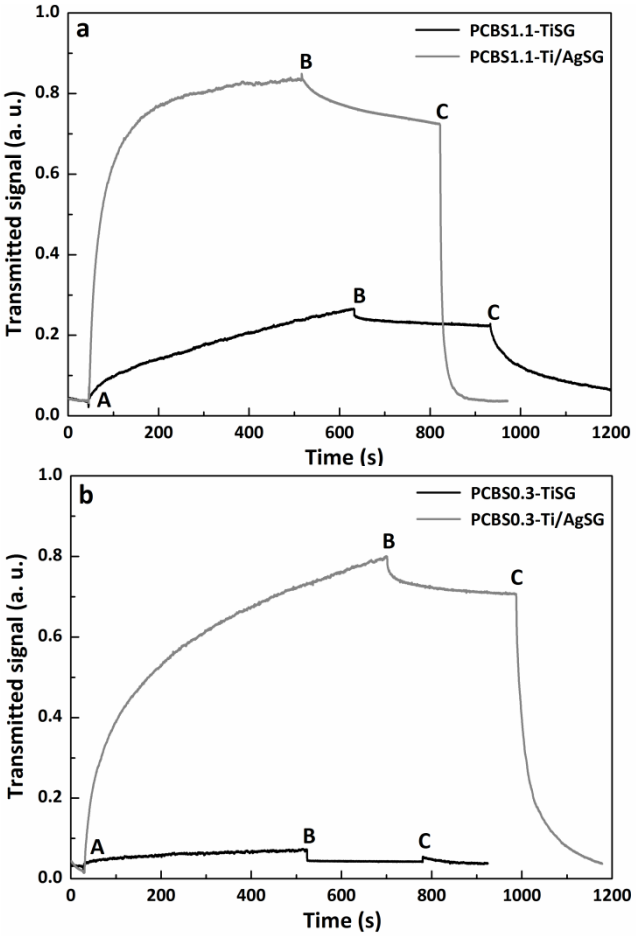

Fig. 10. Writing-relaxing-erasing cycles as a function of time for: (a) PCBS1.1-TiSG and PCBS1.1-Ti/AgSG, and (b) PCBS0.3-TiSG and PCBS0.3-Ti/AgSG.

4. Conclusions

A novel strategy for the fabrication of homogenous hybrid inorganic/organic nanocomposites based on a non-toxic azopolymer and silver-containing TiO_2 nanoparticles with birefringent and semiconductive properties was developed. The strategy was based on the employment of the sol-gel method for generating TiO_2 nanoparticles, and silver-containing TiO_2 nanoparticles by adding $AgNO_3$ precursor.

An enhancement of the thermal stability and glass transition temperature was reached in the silver-containing hybrid nanocomposites as proved by TGA and DSC measurements. Additionally, EFM measurements confirmed that the generated hybrid nanocomposites were completely covered by semiconductive nanoparticles. Therefore, the nanoparticles retained their semiconductive properties in the developed hybrid materials.

The designed hybrid nanocomposites showed different optical behaviors. Increasing the azopolymer concentration the photoorientation rate and the maximum and remaining

birefringence values increased due to the larger number of optically active groups in the nanocomposites and cooperative interactions among them. Moreover, the mutual interactions among azobenzene molecules led to an increase of birefringence in the azopolymer when the irradiation light was turned *off*. In the case of the multifunctional nanocomposites, although it was not noted that the nanoparticles hindered the mobility of azobenzene groups during the orientation process, the interactions among photoactive units might be diminished and the birefringence did not increase after turning *off* the pump beam. In nanocomposites with low concentration of azopolymer and high quantity of sol-gel solution the induced birefringence increased dramatically in the silver-containing samples. This result may be related to the interaction between the silver-containing nanoparticles and the azopolymer, and the surface plasmon resonance of the silver nanoparticles at the wavelength of excitation of the azobenzene molecules.

Finally, modification of titanium oxide nanoparticles with silver also had an effect on the nanocomposites morphology. Silver-containing films were more homogeneous and less rough than those without silver and, in addition, they showed a nanostructured surface. This might also be one of the factors that make the optical and thermal properties of the silver-containing nanocomposites better than those without silver.

Acknowledgements

Financial support from the Basque Government (Grupos Consolidados (IT776-13) and from the Spanish Ministry of Economy and Competitiveness (MINECO) (MAT2012-31675) is gratefully acknowledged. We also wish to acknowledge the 'Macrobehaviour-Mesostructure-Nanotechnology' SGIker unit and Raúl Montero, from 'Laser Facility' SGIker unit, for their technical support. A. T. thanks the MICINN for Ramón y Cajal program (RYC-2010-05592) and J. G. acknowledges the University of the Basque Country for the grant "Ayuda para la Especialización de Doctores en la UPV/EHU". Finally, this work is dedicated to the memory of Prof. Iñaki Mondragon.

Notes and references

Group 'Materials + Technologies' (GMT), Department of Chemical and Environmental Engineering, Polytechnic School, University of the Basque Country (UPV/EHU), Plaza Europa 1, 20018 Donostia-San Sebastián, Spain.

**Corresponding authors. Tel.: +34 943 017 163; fax: +34 943 017 130*
E-mail addresses: raquel.fernandez@ehu.es (R. F.) and agnieszka.tercjaks@ehu.es (A. T.)

1 T. Todorov, L. Nicolova and N. Tomova, *Appl. Optics*, 1984, **23**, 4309.
2 A. Natansohn and P. Rochon, *Chem. Rev*., 2002, **102**, 4139.
3 K. G. Yager and C. J. Barrett, *J. Photochem. Photobiol. A: Chem.*, 2006, **182**, 250.
4 T. G. Pedersen, P. M. Johansen and H. C. Pedersen, *J. Opt. A: Pure Appl. Opt.*, 2000, **2**, 272.
5 Y. Yu and T. Ikeda, *J. Photochem. Photobiol. C: Photochem. Rev.*, 2004, **5**, 247.
6 S. K. Yesodha, C. K. S. Pillai and N. Tsutsumi, *Prog. Polym. Sci.*, 2004, **29**, 45.
7 R. Fernández, J. A. Ramos, L. Espósito, A. Tercjak and I. Mondragon, *Macromolecules*, 2011, **44**, 9738.
8 Y. Yu, M. Nakano and T. Ikeda, *Nature*, 2003, **425**, 145.
9 K. Ichimura, S.-K. Oh and M. Nakagawa, *Science*, 2000, **288**, 1624.
10 H. S. Lim, W. H. Lee, S. G. Lee, D. Lee, S. Jeon and K. Cho, *Chem. Commun.*, 2010, **46**, 4336.
11 A. Goulet-Hanssens, K. L. W. Sun, T. E. Kennedy and C. J. Barrett, *Biomacromolecules*, 2012, **13**, 2958.
12 Z. Sekkat, J. Wood, E. F. Aust, W. Knoll, W. Volksen and R. D. Miller, *J. Opt. Soc. Am. B*, 1996, **13**, 1713.
13 S.-K. Oh., M. Nakagawa and K. Ichimura, *J. Mater. Chem.*, 2001, **11**, 1563.
14 K. Tawa, K. Kamada, K. Kiyohara, K. Ohta, D. Yasumatsu, Z. Sekkat and S. Kawata, *Macromolecules*, 2001, **34**, 8232.
15 Y. Wu, Y. Demachi, O. Tsutsumi, A. Kanazawa, T. Shiono and T. Ikeda, *Macromolecules*, 1998, **31**, 4457.
16 Y. Wu, Y. Demachi, O. Tsutsumi, A. Kanazawa, T. Shiono and T. Ikeda, *Macromolecules*, 1998, **31**, 349.
17 A. Priimagi, J. Vapaavuori, F. J. Rodriguez, C. F. J. Faul, M. T. Heino, O. Ikkala, M. Kauranen and M. Kaivola, *Chem. Mater*., 2008, **20**, 6358.
18 S. Mann, W. Shenton and M. Li, *Adv. Mater.*, 2000, **12**, 147.
19 Y. N. Xia, P. D. Yang, Y. G. Sun, Y. Y. Wu, B. Mayers, B. Gates, Y. D. Yin and F. Kim, *Adv. Mater.*, 2003, **15**, 353.
20 Z. Tang and N. A. Kotov, *Adv. Mater.*, 2005, **17**, 951.
21 L. Kelly, E. Coronado, L. L. Zhao and G. C. Schatz, *J. Phys. Chem. B*, 2003, **107**, 668.
22 C. Hubert, A. Rumyantseva, G. Lerondel, J. Grand, S. Kostcheev, L. Billot, A. Vial, R. Bachelot, P. Royer, S. H. Chang, S. K. Gray, G. P. Wiederrecht and G. C. Schatz, *Nano Lett.*, 2005, **5**, 615.
23 A. Zhang and Y. Fang, *Chem. Phys.*, 2006, **331**, 55.
24 P. Ahonen, D. J. Schiffrin, J. Paprotny and K. Kontturi, *Phys. Chem. Chem. Phys.*, 2007, **9**, 651.
25 J. Gao, Y. Sun, J. Zhou, Z. Zheng, H. Chen, W. Su and Q. Zhang, *J. Polym. Sci. Part A Polym. Chem.*, 2007, **45**, 5380.
26 B. Vlčková, M. Moskovits, I. Pavel, K. Šišková, M. Sládková and M. Šlouf, *Chem. Phys. Lett.*, 2008, **455**, 131.
27 J. Zhou, J. Yang, Y. Sun, D. Zhang, J. Shen, Q. Zhang and K. Wang, *Thin Solid Films*, 2007, **515**, 7242.
28 S. Wu, J. Shen, J. Huang, Y. Wu, Z. Zhang, Y. Hu, W. Wu, W. Huang, K. Wang and Q. Zhang, *Polymer*, 2010, **51**, 1395.
29 J. Shen, S. Wu, J. Huang, Q. Zhang and K. Wang, *Thin Solid Films*, 2010, **518**, 2128.
30 S. Yang, Y. Horibe, C.-H. Chen, P. Mirau, T. Tatry, P. Evans, J. Grazul and E. M. Dufresne, *Chem. Mater.*, 2002, **14**, 5173.
31 S. Haseloh, S. Y. Choi, M. Mamak, N. Coombs, S. Petrov, N. Chopra and G. A. Ozin, *Chem. Commun.*, 2004, **13**, 1460.
32 E. B. Cho and K. Char, *Chem. Mater.*, 2004, **16**, 270.
33 Z. Sun and J. S. Gutmann, *Physica A*, 2004, **339**, 80.
34 C. J. Brinker and G. W. Scherer, *Sol-Gel Science*, 1990, New York: Academic.
35 J. Gutierrez, A. Tercjak and I. Mondragon, *J. Am. Chem. Soc.*, 2010, **132**, 873.
36 R. Fernández, I. Mondragon, P. A. Oyanguren and M. J. Galante, *React. Funct. Polym.*, 2008, **68**, 70.
37 M. I. Sarwar, S. Zulfiqar and Z. Ahmah, *J. Sol-Gel Sci. Technol.*, 2007, **44**, 41.
38 T. Boiadjieva, G. Cappelletti, S. Ardizzone, S. Rondinini and A. Vertova, *Phys. Chem. Chem. Phys.*, 2003, **5**, 1689.
39 R. Parra, M. S. Góes, M. S. Castro, E. Longo, P. R. Bueno and J. A. Varela, *Chem. Mater*., 2008, **20**, 143.
40 S. S. Mahapatra and N. Karak, *Mater. Chem. Phys.*, 2008, **112**, 1114.
41 U. Chatterjee, S. K. Jewrajka and S. Guha, *Polym. Composites*, 2009, **30**, 827.
42 Q. Shi, N. Vitchuli, J. Nowak, J. Noar, J. M. Caldwell, F. Breidt, M. Bourham, M. McCord and X. Zhang, *J. Mater. Chem.*, 2011, **21**, 10330.
43 Y. Sun, Z. Zhang, K.-S. Moon and C. P. Wong, *J. Polym. Sci.: Part B: Polym. Phys.*, 2004, **42**, 3849.
44 C. Noguez, *J. Phys. Chem. C*, 2007, **111**, 3806.

45 A. Dhanabalan, C. R. Mendonca, D. T. Balogh, L. Misoguti, C. J. L. Constantino, J. A. Giacometti, S. C. Zilio and O. N. Oliveira Jr., *Macromolecules*, 1999, **32**, 5277.
46 S. Gimeno, P. Forcén, L. Oriol, M. Piñol, C. Sánchez, F. J. Rodríguez, R. Alcalá, K. Jankova and S. Hvilsted, *Eur. Polym. J.*, 2009, **45**, 262.